Facet Stability in Oxygen-Induced Nanofaceting of Re(12$\bar{3}$1)

Hao Wang,[†] Ally S. Y. Chan,[†,§] Wenhua Chen,[†] Payam Kaghazchi,[‡] Timo Jacob,[‡] and Theodore E. Madey[†,*]

[†]Department of Physics and Astronomy and Laboratory for Surface Modification, Rutgers, The State University of New Jersey, 136 Frelinghuysen Road, Piscataway, New Jersey 08854, and [‡]Fritz-Haber-Institut der Max-Planck-Gesellschaft, D-14195 Berlin, Germany. [§]Present address: UOP LLC, 25 E. Algonqin Rd., Des Plaines, IL 60017.

ARTICLE

ABSTRACT The stability of the various facets in oxygen-induced faceting of Re(12$\bar{3}$1) has been studied by low-energy electron diffraction, scanning tunneling microcopy, and synchrotron-based high-resolution X-ray photoemission spectroscopy. When Re(12$\bar{3}$1) is annealed at 800–1200 K in oxygen (10^{-7} Torr), the surface becomes completely covered with nanometer-scale facets, and its morphology depends on the substrate temperature and oxygen exposure. Especially, the (11$\bar{2}$1) facet competes with the (10$\bar{1}$1) facet in determining the surface morphology, and the stability of each facet relies on oxygen coverage. Using density functional theory, the O—Re binding energies on the facets for various oxygen concentrations are calculated to explain how the oxygen coverage affects the anisotropy of surface free energy, which in turn determines the morphology of the faceted surface.

KEYWORDS: rhenium · faceting · oxygen · scanning tunneling microscopy · low-energy electron diffraction · photoemission spectroscopy · chemisorption · oxidation

Adsorbate-induced faceting of surfaces, driven by the anisotropy of surface free energy, is a general phenomenon observed in many systems.[1–3] Usually the facets have more close-packed surface structures than the original surface, resulting in a minimized surface free energy although the total surface area may be increased. Studies of adsorbate-induced faceting can deepen our understanding of the stability of surfaces under reactive gas environment, which is essential for selecting and controlling a desired surface morphology. Faceted surfaces have also been used as model systems to study structural sensitivity in catalytic reactions[4–6] and may be used as templates to grow nanostructures.[7,8]

Previous studies of adsorbate-induced faceting of metal surfaces focus mainly on body-centered cubic or face-centered cubic metals, such as W(111),[1,2] Mo(111),[9,10] Ni(210),[11,12] Pt(210),[13] Ir(210),[14] Rh(553),[15] and vicinal Cu surfaces.[16–19] For Re, a hexagonal close-packed (hcp) metal, little is known about its faceting behavior although it is an important component of many catalysts.[20–22] Recently we have reported a complex morphological evolution of faceting on Re(12$\bar{3}$1) when the surface is covered by oxygen at 300 K and annealed at $T > 700$ K.[23,24] As shown in Figure 1a,b, the Re(12$\bar{3}$1) surface is atomically rough, with six layers of atoms exposed; it has relatively high surface free energy and high probability to form facets when covered by certain adsorbates and annealed. The morphology of the faceted surface depends on the initial oxygen coverage on Re(12$\bar{3}$1), and the evolution of facets is believed to be induced by the change of surface energy anisotropy due to adsorption of oxygen. When oxygen coverage (θ) is between 0.7 monolayer (ML) and 0.9 ML, long ridges formed by (01$\bar{1}$0) and (11$\bar{2}$1) facets emerge on Re(12$\bar{3}$1) upon annealing;[23] here 1 ML refers to the saturation coverage of oxygen at 300 K. According to an early measurement of oxygen adsorption on another reactive transition metal surface, W(100),[25] the approximate limit of oxygen concentration imposed by room-temperature exposure to Re(12$\bar{3}$1) can be estimated as $\sim 1 \times 10^{15}$ cm^{-2}. For 0.9 ML $< \theta <$ 1 ML, the ridges become truncated by a third facet, (10$\bar{1}$0), which has the same surface structure as (01$\bar{1}$0) but a higher tilt angle with respect to (12$\bar{3}$1).[23] When Re(12$\bar{3}$1) is fully covered by oxygen (θ = 1 ML), a fourth facet, (01$\bar{1}$1), also emerges upon annealing.[23] The spatial relationship between Re(12$\bar{3}$1) and all the observed facets is shown in the stereographic projection plot of the hcp lattice in Figure 1c. It is not surprising that (01$\bar{1}$0), (10$\bar{1}$0), and (01$\bar{1}$1) appear as facets because they all have rather smooth surfaces and thus low surface free energies. However, the last facet that forms, (11$\bar{2}$1), is atomically rough, with four layers of atoms exposed; this raises the question of why it appears as

*Address correspondence to madey@physics.rutgers.edu.

Received for review September 17, 2007 and accepted November 01, 2007.

Published online November 29, 2007.
10.1021/nn700238r CCC: $37.00

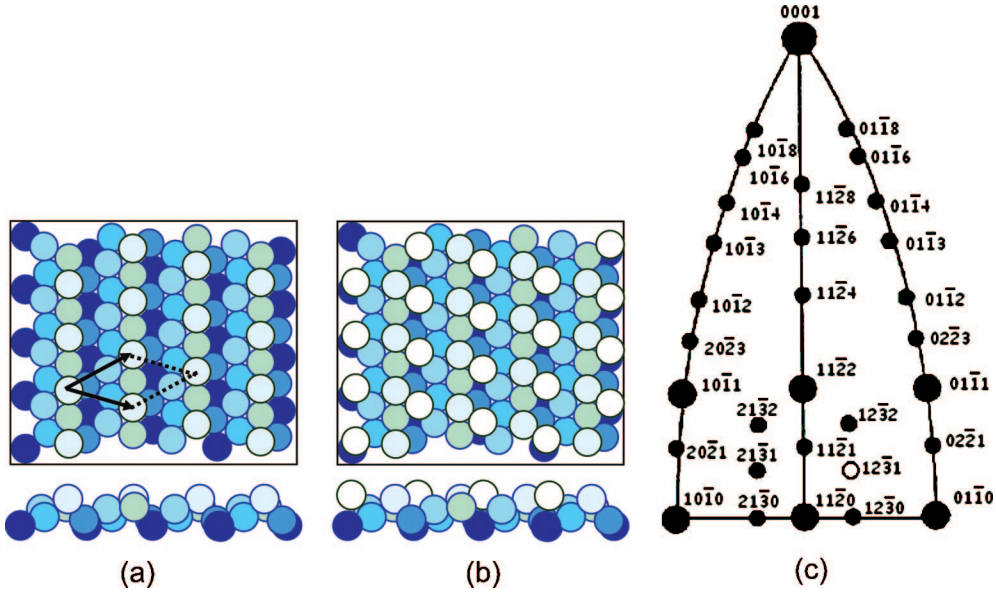

Figure 1. (a,b) Ball models of the Re(12$\bar{3}$1) surface showing two different stacking sequences. A unit cell is also labeled in (a). (c) Stereographic projection of the hcp lattice on the (11$\bar{2}$0) plane. The (12$\bar{3}$1) surface is labeled by a hollow circle.

a facet. One clue lies in the experimental observation that the surface area occupied by (11$\bar{2}$1) decreases when the initial oxygen coverage increases,[23] indicating that the (11$\bar{2}$1) facet may be metastable if oxygen coverage exceeds the limit imposed by oxygen adsorption at 300 K.

In this paper we build upon our previous work[23] and demonstrate that the stability of the (11$\bar{2}$1) facet indeed relies on surface oxygen concentration by investigating the faceting behavior of Re(12$\bar{3}$1) when oxygen is adsorbed at high temperatures. In contrast to the behavior observed for room-temperature adsorption followed by annealing,[23] the (11$\bar{2}$1) facet completely disappears and a new facet, (10$\bar{1}$1), emerges together with the other three facets when Re(12$\bar{3}$1) is exposed to >120 L (1 L (langmuir) = 10^{-6} Torr · s = 1.33×10^{-4} Pa · s) of oxygen between 800 and 1000 K. Only at higher substrate temperatures (>~1200 K) does the (10$\bar{1}$1) facet become unfavorable, and the faceted surface reverts to the previous morphology including the (11$\bar{2}$1) facet. Our results demonstrate the complexity of surface morphology in adsorbate-induced faceting of hcp metal surfaces and have important implications for Re-based catalysts that operate under oxygen-rich conditions since the structures of the catalysts often affect their performance.

RESULTS

Figure 2a shows a typical low-energy electron diffraction (LEED) pattern from a fully faceted surface prepared by dosing 120 L O_2 at 300 K, followed by annealing at 900 K. None of the LEED spots converges to the screen center when the incident electron energy (E_e) increases, indicating the surface is completely faceted. This LEED pattern is almost the same as that in our previous report, where the surface was prepared by dosing 10 L O_2 (θ = 1 ML) at 300 K, followed by annealing at 1000 K.[23] Following the procedure described in ref 23, we can identify representative but relatively weak spots from (11$\bar{2}$1) facets as marked by arrows in Figure 2a. However, when the same amount of O_2 (120 L) is dosed at 900 K, the LEED pattern changes: LEED spots from the (11$\bar{2}$1) facets completely disappear, and more streaky features appear (see Figure 2b). Some of the new streaky features (two examples labeled by arrows in Figure 2b) also do not move toward the converging centers of the facets seen in Figure 2a as E_e is changed, indicating the formation of new facets.

The morphological changes can be better revealed in scanning tunneling microscopy (STM) measurements. Figure 3a is a typical STM image taken from a faceted surface prepared by dosing 120 L O_2 at 300 K, followed by annealing at 900 K. The morphology is the same as reported before: four different facets of orientations (11$\bar{2}$1), (01$\bar{1}$0), (01$\bar{1}$1), and (10$\bar{1}$0) are present.[23] Figure 3b is a typical STM image taken after the Re(12$\bar{3}$1) surface was exposed to 120 L O_2 at 900 K, in which we can identify three of the four facets that appear in Figure 3a. However, a notable difference is that the (11$\bar{2}$1) facet totally disappears and a new facet takes its place. This observation is consistent with the LEED results. Since the area-weighted combinations of all the observed facets must retain the orientation of the macroscopic Re(12$\bar{3}$1) surface, the replacement of (11$\bar{2}$1) by the new facet is accompanied by the rebalancing of the relative amounts of the other three remaining facets; for example, the (01$\bar{1}$0) and (01$\bar{1}$1) facets occupy more surface area per projected unit area on Re(12$\bar{3}$1) in Figure 3b than in Figure 3a. The orientation of the

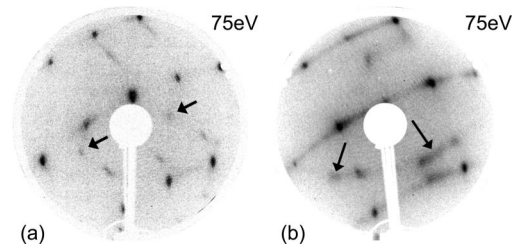

Figure 2. LEED patterns of faceted Re(12$\bar{3}$1) surfaces prepared by (a) dosing 120 L O_2 at 300 K, followed by annealing at 900 K, and (b) dosing 120 L O_2 at 900 K.

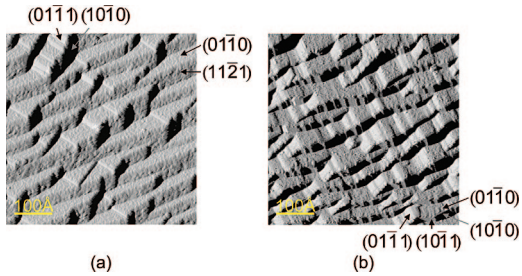

Figure 3. 500 Å × 500 Å STM images of faceted Re(12$\bar{3}$1) surfaces prepared by (a) dosing 120 L O_2 at 300 K, followed by annealing at 900 K, and (b) dosing 120 L O_2 at 900 K.

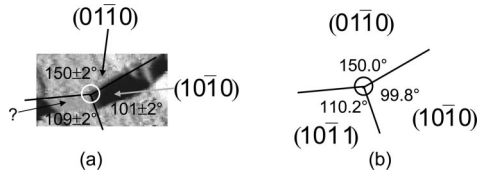

Figure 4. (a) 220 Å × 120 Å STM image showing measurements of the angles between intersection lines of (01$\bar{1}$0), (01$\bar{1}$1), and the new facet. (b) Ideal angle values calculated from the projected intersection lines between (01$\bar{1}$0), (01$\bar{1}$0), and (10$\bar{1}$1) on the (12$\bar{3}$1) surface.

new facet can be identified by measuring the angles between the edge lines of neighboring facets. The results of the angle measurements are shown in Figure 4a, and the only plausible facet that gives good agreement is (10$\bar{1}$1) (see Figure 4b).

This morphological phase transition occurs only in a narrow temperature window. Figure 5a−c shows STM images of the surface morphology after Re(12$\bar{3}$1) was exposed to 360 L O_2 at 800, 1000, and 1200 K, respectively. The average facet size increases with temperature, but the (10$\bar{1}$1) facet only exists when the substrate temperature is between 800 and 1000 K during oxygen exposure. When the sample is heated at 1200 K during oxygen exposure, not only does the (11$\bar{2}$1) facet reemerge, but also the (01$\bar{1}$1) facet almost disappears. Note that in Figure 5c there are many steps on the (11$\bar{2}$1) facets. Although a combination of only (01$\bar{1}$0), (10$\bar{1}$0), and (11$\bar{2}$1) facets cannot retain the macroscopic orientation of the Re(12$\bar{3}$1) (see the stereographic projection in Figure 1c), these steps lead to local effective orientations that deviate from (11$\bar{2}$1) and help retain the macroscopic orientation.

The chemical properties of the faceted Re(12$\bar{3}$1) surfaces prepared under different conditions are investigated by high-resolution X-ray photoemission spectroscopy (HRXPS). Figure 6a shows a Re4$f_{7/2}$ spectrum taken from the faceted Re(12$\bar{3}$1) surface prepared by dosing 10 L O_2 at 300 K, followed by annealing at 1000 K. Besides the Re bulk peak at 40.3 eV, the Re4$f_{7/2}$ spectrum shows distinct features on the higher binding energy side that reflect Re4$f_{7/2}$ surface core level shifts (SCLS) induced by Re−O bonding in different chemical environments. Four SCLS components are needed to fit the Re4$f_{7/2}$ spectrum satisfactorily, and details of the fitting procedure have been described elsewhere.[24,26] The components labeled as 1, 2, and 3 in Figure 6a correspond to SCLS of 0.22, 0.45, and 0.73 eV, respectively; they are assigned to surface Re atoms bonded to one, two, and three O atoms on the basis of similar shifts measured on the p(2×1)-O/Re(0001) surface.[27] The component with a 1.03 eV binding energy shift is attributed to the formation of a surface oxide ReO by comparing the shift with those for Re oxides and assuming that core level shifts are additive for oxidation states.[28] Similar binding energy shifts (1–1.1 eV) observed on O-covered polycrystalline Re[29] and Re(0001)[27] surfaces are also attributed to the formation of ReO.

When the Re(12$\bar{3}$1) surface is exposed to 300 L O_2 at 1000 K, the Re4$f_{7/2}$ spectrum changes drastically (see Figure 6b); not only does the ReO component become dominant among surface peaks, but also an extra peak with SCLS of 1.68 eV emerges. This new peak is attributed to the formation of a new surface oxide species, Re_2O_3.[29] By comparing the Re4$f_{7/2}$ spectra in Figure 6a, it is clear that the surface oxygen concentration upon adsorption at high temperature is larger than that upon room-temperature adsorption, which may be the key factor that causes the morphological change.

DISCUSSION

Faceting is believed to be thermodynamically driven by the anisotropy of surface free energy but limited by kinetic factors such as nucleation and diffusion.[3,30] When surfaces are covered by thin layers of chemisorbed molecules/atoms, not only do their surface free energies decrease due to the energy release from the chemical binding process, but also the anisotropy of the surface free energy changes. This originates from different adsorbate binding energies on inequivalent surfaces, associated with variations in bonding geometry. Apparently, the adsorption coverage (cm^{-2}) of available molecules/atoms and their chemical states are important in determining the surface energy anisotropy and the morphology of the faceted surface. For the O/Re(12$\bar{3}$1) surface, we have demonstrated that the

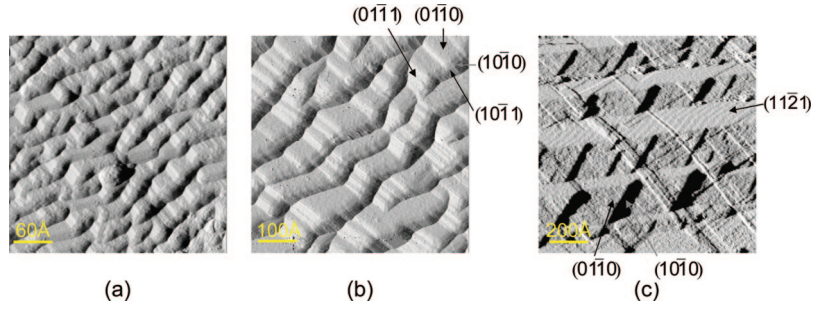

Figure 5. STM images of faceted Re(12$\bar{3}$1) surfaces prepared by dosing 360 L O_2 at different temperatures: (a) 800 K, 300 Å × 300 Å; (b) 1000 K, 500 Å × 500 Å; (c) 1200 K, 1000 Å × 1000 Å.

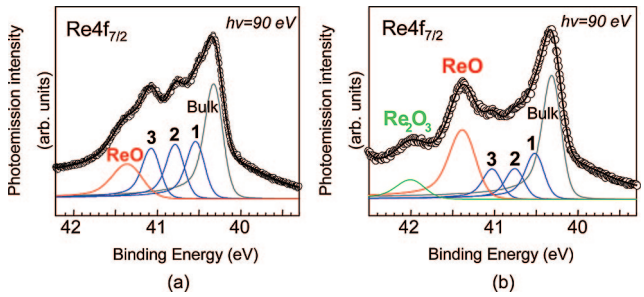

Figure 6. HRXPS spectra of $Re4f_{7/2}$ taken with normal emission angle from surfaces prepared by (a) dosing 10 L O_2 ($\theta = 1$ ML), followed by annealing at 1000 K, and (b) dosing 300 L O_2 at 1000 K. The photon energy is 90 eV. The peak components labeled as 1, 2, and 3 correspond to Re atoms bonded to one, two, and three O atoms, respectively. The peak components for Re bulk and surface oxides ReO and Re_2O_3 are also labeled.

morphology of the faceted surface upon annealing in a vacuum at $T > 700$ K evolves as the initial oxygen coverage at 300 K increases.[23] In this process, the atomically rough $(11\bar{2}1)$ surface always appears as a facet, although it occupies less surface area when the oxygen initial coverage increases. An important characteristic of the $(11\bar{2}1)$ facet is that it has the smallest tilt angle (12.0°) with respect to the $(12\bar{3}1)$ substrate among all the facets observed. So, for other facets that have tilt angles higher than 12.0°, to replace $(11\bar{2}1)$, not only must they have a lower surface free energy than $(11\bar{2}1)$, but the energy must be low enough to compensate the higher surface area creation.

When the surface is exposed to oxygen at 300 K, the maximum coverage of available oxygen atoms is limited by the density of adsorption sites on the planar $Re(12\bar{3}1)$ surface. Here we neglect the possibility of oxygen diffusing into the bulk because the exposure is moderate (<360 L). To explore possible morphological changes beyond this limit, one can anneal the $Re(12\bar{3}1)$ surface in an oxygen atmosphere so that some facets may become energetically unfavorable and undergo further faceting; our results show that $(11\bar{2}1)$ is such a facet. Upon dosing oxygen at high substrate temperatures, the total concentration of adsorbed oxygen atoms can exceed 1 ML and is controlled by both the total oxygen exposure and the substrate temperature; the latter affects the balance of oxygen adsorption, oxidation, and desorption. The fact that the $(11\bar{2}1)$ facet disappears at 800–1000 K and reemerges at ~1200 K (Figure 5) gives strong evidence that the instability of $(11\bar{2}1)$ is induced by adsorbed oxygen atoms exceeding some critical concentration.

Since the main morphological difference between the faceted surfaces prepared by dosing oxygen at different temperatures is whether $(11\bar{2}1)$ or $(10\bar{1}1)$ appears, we first focus the discussion on how their surface energies can be affected by oxygen adsorption. Using density functional theory (DFT) calculations, we find the surface energies of clean $(10\bar{1}1)$ and $(11\bar{2}1)$ are very close: $\gamma^{clean}_{(10\bar{1}1)} = 2.13 \times 10^{15}$ eV · cm^{-2} and $\gamma^{clean}_{(11\bar{2}1)} = 2.20 \times 10^{15}$ eV · cm^{-2}. The calculated energies are in good agreement with the experimental value of the average surface energy for Re surfaces, which is about 2.3×10^{15} eV · cm^{-2}.[31,32] However, since the tilt angle of $(10\bar{1}1)$ with respect to $(12\bar{3}1)$ is 41.7°, much higher than that of $(11\bar{2}1)$ (12.0°), the surface energy per projected unit area on $(12\bar{3}1)$ for clean $(10\bar{1}1)$ is much larger than that for clean $(11\bar{2}1)$. The surface energy difference $\Delta\gamma_1$ due to this tilt angle effect can be estimated as

$$\Delta\gamma_1 = \frac{\gamma^{clean}_{(10\bar{1}1)}}{\cos 41.7°} - \frac{\gamma^{clean}_{(11\bar{2}1)}}{\cos 12.0°} = 0.60 \times 10^{15}\ \text{eV·cm}^{-2} \quad (1)$$

When both $(11\bar{2}1)$ and $(10\bar{1}1)$ are covered by low oxygen concentrations, $(11\bar{2}1)$ is still favored against $(10\bar{1}1)$. Figure 7 shows oxygen binding energies on $Re(11\bar{2}1)$, $Re(10\bar{1}1)$, and $Re(01\bar{1}0)$ for different oxygen concentrations per projected unit area on $(12\bar{3}1)$ based on our DFT calculations. For a given oxygen concentration, an increase in oxygen binding energy correlates with a decrease in surface free energy. Clearly in Figure 7, even when the oxygen concentration is as high as $\sim 1 \times 10^{15}$ cm^{-2}, the approximate limit of oxygen concentration imposed by room-temperature exposure to $Re(12\bar{3}1)$, the O−Re binding energy difference for $Re(10\bar{1}1)$ and $Re(11\bar{2}1)$ is only about 0.2 eV · atom^{-1}, not enough to offset the initial surface energy advantage of $Re(11\bar{2}1)$. However, when oxygen concentration is further increased by formation of surface oxides at higher sample temperature, the O−Re binding energy difference for $Re(10\bar{1}1)$ and $Re(11\bar{2}1)$ may increase and eventually cause $Re(10\bar{1}1)$ to be more favorable. In Figure 7, when the oxygen concentration is about 2×10^{15} cm^{-2}, the O−Re binding energy difference for $Re(10\bar{1}1)$ and $Re(11\bar{2}1)$ is increased to 0.5 eV · atom^{-1}. Therefore, the binding energy difference per projected unit area on $(12\bar{3}1)$ is 1×10^{15} eV · cm^{-2}, which is more than enough to overcome the initial surface energy advantage of $Re(11\bar{2}1)$ and to trigger the formation of $(10\bar{1}1)$ facets. Although the above discussion is confined to the $T = 0$ K limit and does not include the effects of back-

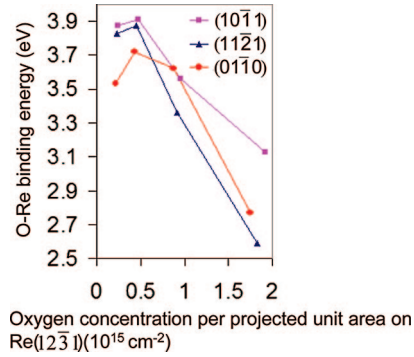

Figure 7. Oxygen binding energies on $Re(11\bar{2}1)$, $(10\bar{1}1)$, and $(01\bar{1}0)$ as functions of oxygen concentration per projected unit area on $(12\bar{3}1)$. The O−Re binding energies are referenced to gas-phase O_2.

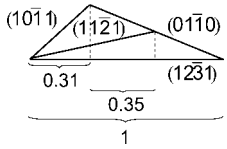

Figure 8. Cross sections of ridges formed by (11$\bar{2}$1) and (01$\bar{1}$0) as well as by (10$\bar{1}$1) and (01$\bar{1}$0).

ground oxygen pressure and substrate temperature on surface free energy, it already shows the importance of oxygen concentration in determining the surface morphology of faceted Re(12$\bar{3}$1).

When the (11$\bar{2}$1) facet is replaced by the (10$\bar{1}$1) facet, the relative surface areas occupied by the other three remaining facets must also change to retain the macroscopic orientation of the Re(12$\bar{3}$1) surface. Here we illustrate qualitatively that even after considering energetic contributions from the remaining facets, the removal of (11$\bar{2}$1) still does not occur at low oxygen concentrations. Because among the three remaining facets, (01$\bar{1}$0) has both the most close-packed surface structure and the smallest tilt angle (22.1°) to (12$\bar{3}$1), we neglect the (10$\bar{1}$0) and (01$\bar{1}$1) facets and focus on the effect of (01$\bar{1}$0). We do this by comparing the surface energy of a ridge formed by (11$\bar{2}$1) and (01$\bar{1}$0) (type I) with that of a ridge formed by (10$\bar{1}$1) and (01$\bar{1}$0) (type II). The cross sections of these two types of ridges are shown in Figure 8, and the structural transition from the first to the second type of ridge can be regarded as follows: 31% of the projected area on (12$\bar{3}$1) that is originally occupied by (11$\bar{2}$1) gets replaced by (10$\bar{1}$1), 35% of the projected area on (12$\bar{3}$1) that is also originally occupied by (11$\bar{2}$1) gets replaced by (01$\bar{1}$0), and the remaining 34% of the projected area on (12$\bar{3}$1) that is originally occupied by (01$\bar{1}$0) is intact. The surface energy of clean (01$\bar{1}$0) is $\gamma^{clean}_{(01\bar{1}0)} = 1.83 \times 10^{15}$ eV · cm^{-2} from our DFT calculations, so the surface energy difference $\Delta\gamma_2$ per projected unit area on (12$\bar{3}$1) between clean (01$\bar{1}$0) and (11$\bar{2}$1) due to the tilt angle effect can be estimated as

$$\Delta\gamma_2 = \frac{\gamma^{clean}_{(01\bar{1}0)}}{\cos 22.1°} - \frac{\gamma^{clean}_{(11\bar{2}1)}}{\cos 12.0°} = -0.27 \times 10^{15}\ \text{eV·cm}^{-2} \quad (2)$$

When the surface is clean, the energy difference per projected unit area on (12$\bar{3}$1) between type II and type I ridges is

$$\Delta E = 0.31\Delta\gamma_1 + 0.35\Delta\gamma_2 = 0.09 \times 10^{15}\ \text{eV·cm}^{-2} > 0 \quad (3)$$

Therefore, a type I ridge formed by (11$\bar{2}$1) and (01$\bar{1}$0) is favored against a type II ridge formed by (01$\bar{1}$1) and (01$\bar{1}$0) if faceting ever occurs on the clean surface. This situation does not change when the surface is covered by low oxygen concentrations ($<0.5 \times 10^{15}$ cm^{-2}) because ΔE remains positive due to the following reasons: any change in $\Delta\gamma_1$ is very small because the O−Re binding energies on (10$\bar{1}$1) and (11$\bar{2}$1) are comparable, while $\Delta\gamma_2$ increases because the O−Re binding energy on (01$\bar{1}$0) is much less than that on (11$\bar{2}$1) at low oxygen concentrations (see Figure 7). When the oxygen concentration per projected unit area on (12$\bar{3}$1) is about 1×10^{15} cm^{-2}, the O−Re binding energies on (01$\bar{1}$0) and (10$\bar{1}$1) both become ~0.2 eV · atom^{-1} more than that on (11$\bar{2}$1), so $\Delta\gamma_1$ and $\Delta\gamma_2$ are changed to 0.4×10^{15} and -0.47×10^{15} eV · cm^{-2}, respectively. If we put the new values of $\Delta\gamma_1$ and $\Delta\gamma_2$ into eq 3, the energy difference per projected unit area on (12$\bar{3}$1) between type II and type I ridges is now slightly negative ($\Delta E = -0.04 \times 10^{15}$ eV · cm^{-2}) and is enough to trigger the structural transition of the ridge from type I to type II. Considering the uncertainties in the O−Re binding energies and the fact that 1×10^{15} cm^{-2} is only a rough estimation of the saturation oxygen coverage on Re(12$\bar{3}$1) at 300 K, the small total energy gain (~0.04×10^{15} eV · cm^{-2}) from the structural transition of the ridge suggests that the oxygen saturation coverage on Re(12$\bar{3}$1) at 300 K is close to the critical oxygen concentration necessary for complete removal of the (11$\bar{2}$1) facet. When the oxygen concentration per projected unit area on (12$\bar{3}$1) is increased further to ~2×10^{15} cm^{-2}, both the (01$\bar{1}$0) and (10$\bar{1}$1) facets become energetically favorable against the (11$\bar{2}$1) facet, which is consistent with the experimental observation that the (11$\bar{2}$1) facet disappears at high oxygen concentrations.

When the Re(12$\bar{3}$1) surface is exposed to 300 L O_2 at 1000 K (see Figure 6b), the HRXPS data show the formation of ReO and Re_2O_3 but no other Re oxides with higher oxidation states such as ReO_3 and Re_2O_7. Since both ReO_3 and Re_2O_7 are volatile at 1000 K, one should consider the possibility that the new faceted surface morphology is due mainly to surface etching by oxygen; for various reasons we believe this is not the case. Jacobson and colleagues studied the Re/O interactions at elevated temperatures in high-pressure O/Ar mixtures and found that the Re weight loss due to oxidation at 1300 K with an oxygen partial pressure of 0.2 Torr is about 0.025 mg · cm^{-2} · min^{-1}.[33] In our study, the average depth of the trench formed by (01$\bar{1}$0) and (11$\bar{2}$1) is $h \approx 40$ Å after the Re(12$\bar{3}$1) surface is heated at 1200 K in oxygen (3×10^{-7} Torr) for 20 min; if removal of ReO_x is the cause, the etching rate could be estimated as $\rho h/2t = 2.1 \times 10^{-4}$ mg · cm^{-2} · min^{-1}, where ρ is the bulk density of Re and t is the heating time. Since the oxygen pressure used in our study is about 6 orders smaller than that in Jacobson's study, and our maximum temperature is 100 K lower than Jacobson's, it is unlikely that the assumed etching rate is only 2 orders smaller; the morphological change upon oxygen exposure at high temperature is attributed to surface diffusion of Re rather than etching by sublimation of ReO_x.

CONCLUSION

The surface morphology is very complex in oxygen-induced nanofaceting of Re(12$\bar{3}$1): five different facets with orientations of (11$\bar{2}$1), (01$\bar{1}$0), (10$\bar{1}$0), (01$\bar{1}$1), and (10$\bar{1}$1) are observed under different conditions. Only the first four facets appear when faceting is induced by saturation adsorption of oxygen ($\theta = 1$ ML) at room temperature, followed by annealing at $T > 700$ K. However, unlike (01$\bar{1}$0), (10$\bar{1}$0), and (01$\bar{1}$1), (11$\bar{2}$1) becomes unstable when Re(12$\bar{3}$1) is exposed to oxygen (120–360 L) at 800–1000 K. Evidence of ReO and Re_2O_3 formation is found in this temperature region, which is believed to further increase the surface energy anisotropy and lead to the replacement of (11$\bar{2}$1) by the fifth facet, (10$\bar{1}$1). The (11$\bar{2}$1) facet reemerges when Re(12$\bar{3}$1) is exposed to oxygen at 1200 K and is attributed to reduced oxygen coverage at this temperature. Surface etching by oxidation under our experimental conditions does not appear to play a major role in determining the final surface morphology. Our DFT calculations reveal the importance of adsorbate coverage in determining the surface morphology by affecting the anisotropy of surface free energy.

EXPERIMENTAL AND COMPUTATIONAL PROCEDURES

All the LEED and STM experiments are performed in an ultra-high-vacuum (UHV) chamber with base pressures about 1×10^{-10} Torr. The chamber contains LEED, Auger electron spectroscopy (AES) instrumentation, a quadrupole mass spectrometer (QMS), and a McAllister scanning tunneling microscope. A Re(12$\bar{3}$1) single crystal with a purity of 99.99% is used in the study; it is ~10 mm in diameter, ~1.5 mm thick, and aligned within 0.5° of the (12$\bar{3}$1) orientation. The Re crystal is cleaned by cycles of e-beam heating in oxygen (1×10^{-7} Torr), followed by flashing to above 2000 K, and the cleanliness of the Re surface is checked by the AES. The residual contaminant species such as carbon and oxygen are below 1–2% of a monolayer of atoms. Oxygen is dosed onto the Re surface by backfilling the chamber, and pressures are measured using an uncalibrated Bayard−Alpert ionization gauge. The sample temperatures are measured by an infrared pyrometer.

The occurrence of faceting can be quickly identified by LEED on the basis of the principle that when E_e increases, the diffraction beams from the planar substrate converge to the specular (0,0) beam usually located in the center of the screen, while the diffraction beams from a facet converge to its specular beam position that is generally found considerably displaced from the screen center. All STM measurements are made at room temperature, with a typical sample bias between 0.5 and 1.2 V and a tunneling current between 0.6 and 1 nA. The *X* and *Y* dimensions of the STM scan range are calibrated using atomically resolved STM images of the S(4×4)/W(111) reconstruction,[34] and the *Z* dimension is calibrated on the basis of tilt angle measurements between (211) and (111) planes in faceted O/W(111).[35] The STM images are presented in the differential mode to enhance details of the facets: the measured height variation is differentiated along the *X* direction, and regions having the same *X*-slope are represented by the same gray color. The HRXPS measurements are conducted on beamline U4A of the National Synchrotron Light Source (NSLS) at Brookhaven National Laboratory.[36] The UHV end-station chamber is equipped with a VSW 100 mm hemispherical analyzer operating at a pass energy of 2 eV, and the total instrumental resolution is about 150 meV.

The O−Re binding energies on several Re surfaces are calculated by DFT using the CASTEP code.[37] Throughout the calculations, optimized Vanderbilt-type ultrasoft pseudopotentials[38] and the generalized gradient approximation (GGA) exchange-correlation functional suggested by Perdew, Burke, and Ernzerhof (PBE)[39] are used. Re(10$\bar{1}$1), (01$\bar{1}$0), and (11$\bar{2}$1) surfaces are represented by 14-layer, 11-layer, and 19-layer slabs with ~13 Å vacuum, respectively. For each system, the bottom four layers are fixed at the calculated bulk-crystal structure, and the remaining Re atoms and the adsorbates are allowed to relax freely. For the oxygen-adsorbed system, the cutoff energy is converged to 380 eV, and the Brillouin zone (BZ) sampling of the 1×1 unit cell is converted to 4×4, 5×8, and 4×8 Monkhorst−Pack meshes for Re(11$\bar{2}$1), (01$\bar{1}$0), and (10$\bar{1}$1), respectively.[40]

Acknowledgment. This work has been supported by the U.S. Department of Energy, Office of Basic Energy Sciences.

REFERENCES AND NOTES

1 Madey, T. E.; Guan, J.; Nien, C.-H.; Dong, C.-Z.; Tao, H.-S.; Campbell, R. A. Faceting Induced by Ultrathin Metal Films on W(111) and Mo(111): Structure, Reactivity, and Electronic Properties. *Surf. Rev. Lett.* **1996**, *3*, 1315–1328.

2 Madey, T. E.; Nien, C.-H.; Pelhos, K.; Kolodziej, J. J.; Abdelrehim, I. M.; Tao, H.-S. Faceting Induced by Ultrathin Metal Films: Structure, Electronic Properties and Reactivity. *Surf. Sci.* **1999**, *438*, 191–206.

3 Chen, Q.; Richardson, N. V. Surface Factetting Induced by Adsorbates. *Prog. Surf. Sci.* **2003**, *73*, 59–77.

4 Chen, W.; Ermanoski, I.; Wu, Q.; Madey, T. E.; Hwu, H. H.; Chen, J. G. Adsorption and Decomposition of Acetylene on Planar and Faceted Ir(210). *J. Phys. Chem. B* **2003**, *107*, 5231–5242.

5 Chen, W.; Ermanoski, I.; Madey, T. E. Decomposition of Ammonia and Hydrogen on Ir Surfaces: Structure Sensitivity and Nanometer-Scale Size Effects. *J. Am. Chem. Soc.* **2005**, *127*, 5014–5015.

6 Chen, W.; Ermanoski, I.; Jacob, T.; Madey, T. E. Structure Sensitivity in the Oxidation of CO on Ir Surfaces. *Langmuir* **2006**, *22*, 3166–3173.

7 Bachelet, R.; Cottrino, S.; Nahélou, G.; Coudert, V.; A.; Boulle; Soulestin, B.; Rossignol, F.; Guinebretière, R.; Dauger, A. Self-Patterned Oxide Nanostructures Grown by Post-Deposition Thermal Annealing on Stepped Surfaces. *Nanotechnology* **2007**, *18*, 015301.

8 Wang, H.; Reyhan, M.; Madey, T. E., unpublished data.

9 Song, K.-J.; Lin, J. C.; Lai, M. Y.; Wang, Y. L. Faceting Phase Transitions of Mo(111) Induced by Pd, Au and Oxygen Overlayers. *Surf. Sci.* **1995**, *327*, 17–32.

10 Danko, D. B.; Kuchowicz, M.; Kolacziewicz, J. Adsorbate-Induced Surface Rearrangement of the System Pd/Mo(1 1 1). *Surf. Sci.* **2004**, *552*, 111–122.

11 Kirby, R. E.; McKee, C. S.; Roberts, M. W. Low Temperature Oxygen and Activated Nitrogen Faceting of Ni(210) Surfaces. *Surf. Sci.* **1976**, *55*, 725–728.

12 Kirby, R. E.; McKee, C. S.; Renny, L. V. Faceting of Cu(210) and Ni(210) by Activated Nitrogen. *Surf. Sci.* **1980**, *97*, 457–477.

13 Sander, M.; Imbihl, R.; Schuster, R.; Barth, J. V.; Ertl, G. Microfacetting of Pt(210) Induced by Oxygen Adsorption and by Catalytic Co Oxidation. *Surf. Sci.* **1992**, *271*, 159–169.

14 Ermanoski, I.; Pelhos, K.; Chen, W.; Quinton, J. S.; Madey, T. E. Oxygen-Induced Nano-Faceting of Ir(2 1 0). *Surf. Sci.* **2004**, *549*, 1–23.

15 Gustafson, J.; Resta, A.; Mikkelsen, A.; Westerström, R.; Andersen, J. N.; Lundgren, E.; Weissenrieder, J.; Schmid, M.; Varga, P.; Kasper, N. Oxygen-Induced Step Bunching and Faceting of Rh(553): Experiment and Ab Initio Calculations. *Phys. Rev. B* **2006**, *74*, 035401.

16 Knight, P. J.; Driver, S. M.; Woodruff, D. P. Scanning Tunnelling Microscopy Investigation of the Oxygen-Induced Faceting and "Nano-Faceting" of a Vicinal Copper Surface. *Surf. Sci.* **1997**, *376*, 374–388.
17 Vollmer, S.; Birkner, A.; Lucas, S.; Witte, G.; Wöll, Ch. Nanopatterning of Copper (111) Vicinal Surfaces by Oxygen-Induced Mesoscopic Faceting. *Appl. Phys. Lett.* **2000**, *76*, 2686–2688.
18 Reinecke, N.; Taglauer, E. The Kinetics of Oxygen-Induced Faceting of Cu(115) and Cu(119) Surfaces. *Surf. Sci.* **2000**, *454–456*, 94–100.
19 Walko, D. A.; Robinson, I. K. Energetics of Oxygen-Induced Faceting on Cu(115). *Phys. Rev. B* **2001**, *64*, 045412.
20 Yuan, Y.; Liu, H.; Imoto, H.; Shido, T.; Iwasawa, Y. Performance and Characterization of a New Crystalline $SbRe_2O_6$ Catalyst for Selective Oxidation of Methanol to Methylal. *J. Catal.* **2000**, *195*, 51–61.
21 Solymosi, F.; Tolmacsov, P.; Zakar, T. S. Dry Reforming of Propane over Supported Re Catalyst. *J. Catal.* **2005**, *233*, 51–59.
22 Liu, K.; Fung, S. C.; Ho, T. C.; Rumschitzki, D. S. Heptane Reforming over Pt-Re/Al_2O_3: Reaction Network, Kinetics, and Apparent Selective Catalyst Deactivation. *J. Catal.* **2002**, *206*, 188–201.
23 Wang, H.; Chen, W.; Madey, T. E. Morphological Evolution in Oxygen-Induced Faceting of Re(12$\bar{3}$1). *Phys. Rev. B* **2006**, *74*, 205426.
24 Chan, A. S. Y.; Chen, W.; Wang, H.; Rowe, J. E.; Madey, T. E. Methanol Reactions over Oxygen-Modified Re Surfaces: Influence of Surface Structure and Oxidation. *J. Phys. Chem. B* **2004**, *108*, 14643–14651.
25 Madey, T. E. Adsorption of Oxygen on W(100): Adsorption Kinetics and Electron Stimulated Desorption. *Surf. Sci.* **1972**, *33*, 355–376.
26 Chan, A. S. Y.; Wertheim, G. K.; Wang, H.; Ulrich, M. D.; Rowe, J. E.; Madey, T. E. Surface Atom Core-Level Shifts of Clean and Oxygen-Covered Re(12$\bar{3}$1). *Phys. Rev. B* **2005**, *72*, 035442.
27 Ducros, R.; Fusy, J. Core Level Binding Energy Shifts of Rhenium Surface Atoms for a Clean and Oxygenated Surface. *J. Electron Spectrosc. Relat. Phenom.* **1987**, *42*, 305–312.
28 Tysoe, W. T.; Zaera, F.; Somorjai, G. A. An XPS Study of the Oxidation and Reduction of the Rhenium-Platinum System under Atmospheric Conditions. *Surf. Sci.* **1988**, *200*, 1–14.
29 Morant, C.; Galán, L.; Sanz, J. M. X-Ray Photoelectron Spectroscopic Study of the Oxidation of Polycrystalline Rhenium by Exposure to O_2 and Low Energy O^{2+} Ions. *Anal. Chim. Acta* **1994**, *297*, 179–186.
30 Herring, C. Some Theorems on the Free Energies of Crystal Surfaces. *Phys. Rev.* **1951**, *82*, 87–93.
31 Tyson, W. R.; Miller, W. A. Surface Free Energies of Solid Metals: Estimation from Liquid Surface Tension Measurements. *Surf. Sci.* **1977**, *62*, 267–276.
32 de Boer, F. R.; Boom, R.; Mattens, W. C. M.; Miedema, A. R.; Niessen, A. K. *Cohesion in Metals*; North-Holland: Amsterdam, 1988; pp 758.
33 Jacobson, N. S.; Myers, D. J.; Zhu, D.; Humphrey, D. L. Rhenium/Oxygen Interactions at Elevated Temeratures. *Oxid. Met.* **2001**, *55*, 471–480.
34 Nien, C.-H.; Madey, T. E. Surface Reconstructions and Morphological Modifications: Restructuring of W(111) Induced by Sulfur Overlayers. *Surf. Sci.* **1999**, *433–435*, 254–260.
35 Szczepkowicz, A.; Ciszewski, A.; Bryl, R.; Oleksy, C.; Nien, C.-H.; Wu, Q. F.; Madey, T. E. A Comparison of Adsorbate-Induced Faceting on Flat and Curved Crystal Surfaces. *Surf. Sci.* **2005**, *599*, 55–68.
36 Thiry, P.; Bennett, P. A.; Kevan, S. D.; Royer, W. A.; Chaban, E. E.; Rowe, J. E.; Smith, N. V. A 6 M Toroidal-Grating-Monochromator Beam Line for High Momentum-Resolution Photoelectron Spectroscopy. *Nucl. Instrum. Methods Phys. Res. Sect. A* **1984**, *222*, 85–90.
37 Segall, M. D.; Lindan, P. L. D.; Probert, M. J.; Pickard, C. J.; Hasnip, P. J.; Clark, S. J.; Payne, M. C. First-Principles Simulation: Ideas, Illustrations and the Castep Code. *J. Phys.: Condens. Matter* **2002**, *14*, 2717–2744.
38 Vanderbilt, D. Soft Self-Consistent Pseudopotentials in a Generalized Eigenvalue Formalism. *Phys. Rev. B* **1990**, *41*, 7892–7895.
39 Perdew, J. P.; Burke, K.; Ernzerhof, M. Generalized Gradient Approximation Made Simple. *Phys. Rev. Lett.* **1996**, *77*, 3865–3868.
40 Monkhorst, H. J.; Pack, J. D. Special Points for Brillouin-Zone Integrations. *Phys. Rev. B* **1976**, *13*, 5188–5192.